Orientations of Mistaken Point fronds indicate morphology impacted ability to survive turbulence

Vixseboxse[1], Philip B., Kenchington[2], Charlotte G., Dunn[3], Frances S. and Mitchell*[4], Emily G.*

[1]*School of Earth Sciences, University of Bristol, Wills Memorial Building, Queens Road, Bristol BS8 1RJ, UK.*

[2] *Department of Earth Sciences, University of Cambridge, Downing Street, Cambridge, CB2 3EQ, UK.*

[3] *Oxford University Museum of Natural History, Parks Road, Oxford, OX1 3PW, Oxford, UK.*

[4]*Department of Zoology, University of Cambridge, Downing Street, Cambridge, CB2 3EJ, UK.*

**Corresponding author:* pv17454@bristol.ac.uk

ABSTRACT

The Ediacaran organisms of the Mistaken Point E surface have provided crucial insight into early animal communities, including how they reproduced, the importance of Ediacaran height and what the most important factors were to their community dynamics. Here, we use this iconic community to investigate how morphological variation between eight taxa affected their ability to withstand different flow conditions. For each of *Beothukis*, *Bradgatia*, *Charniodiscus procerus*, *Charniodiscus spinosus*, *Plumeropriscum*, *Primocandelabrum* and *Fractofusus* we measured the orientation and length of their stems (if present) and their fronds. We statistically tested each taxon's stem and frond orientation distributions to see whether they displayed a uniform or multimodal distribution. Where multimodal distributions were identified, the stem/frond length of each cohort was tested to

identify if there were differences in size between different orientation groups. We find that *Bradgatia* and *Thectardis* show a bimodal felling direction, and infer that they were felled by the turbulent head of the felling flow. In contrast, the frondose rangeomorphs including *Beothukis, Plumeropriscum, Primocandelabrum*, and the arboreomorphs were felled in a single direction, indicating that they were upright in the water column, and were likely felled by the laminar tail of the felling flow. These differences in directionality suggests that an elongate habit, and particularly possession of a stem, lent greater resilience to frondose taxa against turbulent flows, suggesting that such taxa would have had improved survivability in conditions with higher background turbulence than taxa like *Bradgatia* and *Thectardis*, which lacked a stem and which had a higher centre of mass, which may have fared better in quieter water conditions.

KEYWORDS: Ediacaran, Mistaken Point, Orientations, Turbidite, Rangeomorphs, Arboreomorphs

INTRODUCTION

The Ediacaran macrobiota is a probably polyphyletic assemblage of organisms which appear in the fossil record ~575 million years ago and contain some of the oldest animals in the fossil record (Xiao and Laflamme 2009; Budd and Jensen 2017; Bobrovskiy et al. 2018; Cuthill and Han 2018; Dunn et al. 2018, 2021; Wood et al. 2019). The morphologies of Ediacaran organisms from Newfoundland and the UK have few clear points of homology with living animal lineages or Phanerozoic fossil groups, which has historically limited our understanding of their phylogenetic affinities and hampers our understanding of the functional ecology of these organisms (Liu et al. 2015).

The Ediacaran communities of Eastern Newfoundland are dominated by the perhaps most distinct members of the Ediacaran macrobiota - the sessile, frondose rangeomorphs (Narbonne and Gehling 2003; Narbonne 2005). Rangeomorphs are characterised by a "fractal" branching architecture (Narbonne 2004; Cuthill and Morris 2014), and which increasing data supports as a clade of stem-group eumetazoans (Cuthill and Han 2018; Dunn et al. 2021). Rangeomorphs numerically dominate these late-Ediacaran sea floors, but they lived alongside a number of different groups the most abundant of which are the arboreomorphs (Clapham et al. 2003; Xiao and Laflamme 2009). These are similarly frondose, but unlike the rangeomorphs which can possess many orders of hierarchical branching, Newfoundland arboreomorphs possess only two (Laflamme et al. 2004; Laflamme and Narbonne 2008; Laflamme et al. 2018). Non-frondose fossils are also present, though rare, in these fossil deposits and the most well-known is *Thectardis* a conical to triangular organism sometimes interpreted as a sponge (Clapham et al. 2004; Sperling et al. 2011).

Of these groups, rangeomorphs are not only the most diverse but display the greatest anatomical variation (Shen et al. 2008; Xiao and Laflamme 2009). Some rangeomorphs are

preserved as single fronds (e.g. *Charnia*), but others were bushy (e.g. *Bradgatia*), spindle-shaped (e.g. *Fractofusus*) or arborescent (e.g. *Primocandelabrum*) (Gehling and Narbonne 2007; Bamforth et al. 2008; Flude and Narbonne 2008; Bamforth and Narbonne 2009; Dunn et al. 2019). Rangeomorph branches differentiated directly from one another or from a central stalk (Dunn et al. 2019) and some rangeomorphs additionally exhibited a naked stem which elevated the frond into the water column upright taxa (Laflamme et al. 2012) increasing the dispersal range of offspring (Mitchell and Kenchington 2018). Most rangeomorphs possessed a spheroidal-discoidal holdfast which anchored them within the sediment (Laflamme et al. 2004), attaching the organism to the substrate and from which the stem or frond derived. Previous functional studies have demonstrated that the high surface area of the repeatedly branched frond maximised nutrient or gas exchange (Laflamme et al. 2009; Sperling et al. 2011; Liu et al. 2015). The phylogenetic relationship between frondose rangeomorphs and the coeval arboreomorphs is currently unclear (Dececchi et al. 2017; Cuthill and Han 2018); some have argued that arboreomorphs are members of the Rangeomorpha (Brasier and Antcliffe 2009), but clear anatomical differences between at least some arboreomorphs and rangeomorphs mean that this view is not universally held, with others suggesting that overtly similar gross morphologies may have arisen through convergence (Laflamme et al. 2018). Indeed, in the modern a sessile, frondose bodyplan is found in myriad different groups, such as ferns, corals and cnidarians, and has been acquired through different developmental processes, demostrating that such a bodyplan can be the produce of similar ecologies or function and is not necessarily indicative of close phylogenetic relationship.

Stems were originally thought to facilitate height-driven tiering in Avalonian communities, allowing taller fronds to reach higher-velocity conditions (Ghisalberti et al. 2014), but more recent work has suggested that not all communities were tiered and that increased height may have additionally functioned in offspring dispersal (Mitchell and Kenchington 2018).

87 Thickening of the stem close to the holdfast – optimisation of the stem as a cantilever beam –
88 is observed in cnidarians (Koehl 1977*a*, *b*), and crinoids (Baumiller and Ausich 1996), where
89 it permits orientation of the crown with the aboral surface facing the flow, initiating aboral
90 inflow and recirculation (Dynowski et al. 2016). Rangeomorphs have been documented as
91 showing a basal thickening of the stem and so may have functioned in the same way
92 (Kenchington and Wilby 2017). By examining the different functional ecology of stemmed
93 and non-stemmed organisms, we can investigate what the advantages of stems were in
94 Ediacaran organisms.

95 These fossils are found preserved within turbiditic sequences, under thin layers of ash which
96 blanketed large swathes of sea floor and smothered thousands of macro-organisms in a single
97 event bed (Wood et al. 2003). Communities are exceptionally preserved and provide a near-
98 census record of the benthic communities (Wood et al. 2003). This in-situ preservation,
99 combined with the sessile habit of the organisms, means that detailed spatial ecological
100 analyses can be used to investigate reproductive strategies (Mitchell et al. 2015), taxonomy
101 (Mitchell et al. 2018), community interactions (Mitchell and Butterfield 2018) and
102 evolutionary drivers (Mitchell et al. 2019, 2020), and in this study supplement functional
103 ecology analyses of the organisms.

104 Here, we use statistical analyses of the orientations of 8 taxa from the E surface, Mistaken
105 Point, Newfoundland: *Beothukis*, *Bradgatia*, *Charniodiscus procerus*, *Charniodiscus*
106 *spinosus*, *Plumeropriscum*, *Primocandelabrum*, *Thectardis*, and *Fractofusus*. We determine
107 the extent to which orientation distributions of populations of complete specimens, stems and
108 fronds are randomly, normally and/or uniformly distributed, and how many sub-groups
109 within each population exist. Where taxa exhibit multi-modal orientation distributions, we
110 use random labelling spatial analyses to determine whether there are any spatial patterns to
111 taxa orientations. These analyses enable us to investigate how morphological features, such

as stems and number of folia influenced the stability of these organisms in the ancient oceans and their ability to withstand burial events of differing magnitudes.

GEOLOGICAL SETTING

The Avalon Assemblage records the evolution of deep marine metazoan communities from the ~574 Ma Drook Formation (Matthews et al. 2021), to the late Ediacaran Bradgate Formation (556.6±6.4 Ma, (Noble et al. 2015)). One of the three assemblages originally proposed by Waggoner 2003, it traces the marine margin of the Avalonian Terrane through the British Isles and Newfoundland. In both regions, sedimentation was dominated by turbidite deposition (Wood et al. 2003; Noble et al. 2015). Throughout the Newfoundland succession, there is a transition in tectonic setting and depositional character, from the basin plain setting of the lower Conception Group to the shallowing-upwards slope setting of the upper Conception and St John's groups, with a concomitant increase in depositional energy and rate of deposition and a basinwards progradation of the locus of sedimentation (Wood et al. 2003; Matthews et al. 2021).

The Mistaken Point Formation is dominated by thick-bedded, mud-rich and ashy turbidites, punctuated by tuffaceous horizons (Wood et al. 2003; Ichaso et al. 2007; Matthews et al. 2021). The bed over the E surface has a thin, coarse crystal tuff, a lower graded portion and an upper portion that consists of alternating dark-light bands (above the chlorite-carbonate band; (Fig S4; Matthews et al. 2021). The exact mode of emplacement of the tuffaceous horizons was long thought to be primarily from water-lain ashfall events (where ashy material enters the basin, and gradually settles out through the water column). However, recent work suggests that at least some of these horizons were instead the product of ashy turbidites, and that they contain variable proportions of volcaniclastic (eruptive and/or

unlithified reworked) and epiclastic (lithified and reworked) material (Noble et al. 2015; Kenchington et al. 2018; Matthews et al. 2021).

The mode of emplacement has direct implications for understanding the process that felled the fronds within the palaeocommunities, and therefore their preserved orientations. If the tuffs were water-lain, they are not necessarily associated with a gravity-driven flow, and accordingly the fronds were interpreted as having been felled by basin contour-parallel currents (Wood et al. 2003). However, if the smothering ashes are a product of turbidity flows, then it is likely that the fronds were felled by these same flows (Matthews et al. 2021). In the specific case of the E surface, however, there is no contention that there is a gravity-driven flow origin for the alignment of fronds on the E Surface (F12 of Wood et al. 2003; Matthews et al. 2021).

Gravity flows and their expression in the rock record

Turbidites are the lithological record of deposition via sediment-laden turbidity currents, and exist on a continuum with other gravity-driven flows and their deposits (Haughton et al. 2009; Talling et al. 2012). The lack of evidence of fluvial input, together with the slump horizons that occur throughout the Mistaken Point Formation (Wood et al. 2003), suggests that the source of the flows in the Mistaken Point Formation are more likely to be those dominantly sourced from slope failure (slumping), rather than rivers. Therefore, here we focus only on the former. Gravity flow behaviour, and thus classification, is principally driven by two factors: the fraction of cohesive components within the sediment, and the overall concentration of sediments within the flow (e.g. Haughton et al. 2009). Higher sediment concentrations, and higher fractions of cohesive components (clay minerals and reworked muds), act to dampen turbulence at the sediment-water interfaces (Cantero et al.

158 2012; Talling et al. 2012), and within dilute turbidity currents (Baas and Best 2002; Baas et
159 al. 2009).

160 The coarse tuff immediately above the E surface could be indicative of particle sorting and
161 winnowing within the more turbulent head of the turbidity current (Sparks and Wilson 1983),
162 while the structure within the rest of the bed is consistent with the hybrid flow model of
163 Haughton et al. 2009 (Matthews et al. 2021). On a broad scale, this mixed/hybrid flow
164 interpretation may be reflected in the increased turbidite thickness within the Mistaken Point
165 Formation (previously interpreted as turbidite ponding, (Ichaso et al. 2007)). Surface
166 weathering, synsedimentary and early diagenetic alteration of the volcaniclastic source for the
167 Mistaken Point turbidites would have produced a clay-rich source sediment (cf. Kiipli et al.
168 2007), enhanced by addition of deposition from nepheloid plumes or as hemipelagic fallout
169 (cf. Kenchington et al. 2018). This high clay content and high sediment load would have
170 increased the cohesion within the flow and so dampened its turbulence, potentially generating
171 conditions conducive to internal laminar flow, while dilution of the turbidite head likely
172 brought concentrations below the threshold for a laminar-dominated regime (similar to the
173 high-density turbidity or lower density mixed flows of Haughton et al., 2009), with turbulent
174 conditions within the turbidite head.

175 As a flow moves down a slope, it can change character and concentration, reflected in
176 different depositional products (Houghton et al. 2009). For example, after slumping,
177 entrainment of water rapidly dilutes the head of the turbidite, inhibiting sediment-induced
178 turbulence dampening (Hallworth et al. 1993; Cartigny et al. 2013). In contrast, entrainment
179 of clay-rich material would have the opposite effect. Differential dilution-driven turbulence
180 often manifests as Kelvin-Helmholtz instabilities (Liu and Jiang 2014), wherein turbulent
181 eddies rotate about a horizontal axis orthogonal to the direction of turbidite propagation (see

182 "roll waves" of Cartigny et al. 2013) – important when we are thinking about the processes
183 controlling frond orientation.

184 **MATERIALS AND METHODS**

185 *Data processing*

186 In this study we used mapped data from the E surface given by Mitchell et al. 2019,
187 supplemented with *Fractofusus* data from Clapham et al. 2003. Mitchell et al. LiDAR
188 scanned the E surface using a Faro Focus 330X to ensure spatial accuracy was maintained
189 over large areas. The LiDAR scans resulted in a 3D surface mesh of 1 mm resolution. In
190 order to get sufficient resolution to resolve taxonomic identity, Mitchell et al also laser
191 scanned the E surface using a Faro Scan Arm v6LLP, resulting in surface meshes of ~0.050
192 mm resolution. The high-resolution scanning was done in grids of ~1m x 1m. Due to large
193 file sizes, these high-resolution scans could not all be viewed simultaneously, so control
194 points were marked in each high-resolution scan, and in the LiDAR scan, enabling accurate
195 combination of the high-resolution scans with the LiDAR surface data (performed using
196 Geomagic 2015). A photomap was created by photographing the specimens along a
197 horizontal and vertical grid, then using Agisoft Photoscan software v1.3.5 to create a
198 photogrammetric render of the surface. The LiDAR scan was then imported into Photoscan,
199 and the photographs aligned on the LiDAR scan to ensure large-scale accuracy. An
200 orthomosaic of the surface was produced within Agisoft PhotoScan, from which the data was
201 collected. The combination of LiDAR, LLP and photogrammetry enabled accurate retention
202 of angle data between photographs, with minimal perspective projection distortion (Mitchell
203 et al. 2019). Specimens were binned into 7 morphogroups: *Beothukis* – a unifoliate, spatulate-
204 fronded rangeomorph, with a short – or absent – stem and holdfast (Brasier and Antcliffe
205 2009; Hawco et al. 2020); *Bradgatia* – a multifoliate rangeomorph consisting of up to eight

206 primary branches from a central branching point on an inferred holdfast (Boynton and Ford
207 1995; Flude and Narbonne 2008); *Charniodiscus procerus* – a unifoliate arboreomorph
208 possessing a circular holdfast, elongate stem, and a lanceolate frond (often laterally
209 displaced) without fractal, rangeomorph-style branching (Laflamme et al. 2004);
210 *Charniodiscus spinosus* – a unifoliate arboreomorph with a large ovate frond, lacking
211 rangeomorph-style branching, tipped with an elongate spine, connected to a large holdfast via
212 a short cylindrical stem (Laflamme et al. 2004); *Plumeropriscum* – a multifoliate
213 rangeomorph composed of at least nine primary branches furcating from an elongate
214 cylindrical stem, attached to the substrate by a discoidal holdfast (Mason and Narbonne
215 2016); *Primocandelabrum* – a multifoliate rangeomorph consisting of a large holdfast,
216 elongate stem, and substantial crown composed of three first order branches (Hofmann et al.
217 2008; Kenchington and Wilby 2017) and *Thectardis* – an erect conical taxon lacking
218 evidence of a holdfast (Clapham et al. 2004). We used the size and orientation data from
219 Clapham et al. 2003 for *Fractofusus*, a spindle-shaped rangeomorph (Gehling and Narbonne
220 2007). We identified 18 *Beothukis*, 52 *Bradgatia*, 61 *C. procerus*, 31 *C. spinosus*, 20
221 *Plumeropriscum*, 47 *Primocandelabrum* and 27 *Thectardis* across 85.42m^2 of the E surface
222 bedding plane. We supplemented this data with 1497 *Fractofusus* orientation data from
223 Clapham et al. 2003.

224 *Retrodeformation*

225 The E surface has undergone tectonic deformation so prior to any analyses, retrodeformation
226 needs to be performed to re-engineer the organisms back to their in-death dimensions (Wood
227 et al. 2003). To perform the retrodeformation, we collected the dimensions and orientations
228 of 24 representative, large, discs across the E Surface (Supp. Fig. 1). Utilising a constant area
229 retrodeformation method, the principle axis lengths for each disc were extracted. Following
230 the methodology of Mitchell et al. (2015), a regression was fitted to determine the

231 retrodeformation ratio (1.75, which within the confidence interval (1.71±0.08) of Mitchell et
232 al. (2015)), which was applied across the entire E surface. To apply this retrodeformation,
233 the annotated photosquares were aligned and stitched together in Inkscape v0.92.4, and
234 rotated to align the principal axes of the mean disc with the vertical and horizontal axes of the
235 document – thus aligning the eigenvectors of retrodeformation with the axes of the document.
236 From here, constant area retrodeformation can be characterised as a deformation, which can
237 be achieved with shortening and elongation of the vertical and horizontal axes. The
238 retrodeformed surface was then rotated to the original orientation. Overall, the photosquares
239 were shortened by 26.7% along the eigenvector oriented 78.5°, and elongated 36.8% along
240 the orthogonal eigenvector of 168.5° (Supp. Fig. 1). We note that, whilst retrodeformation
241 techniques have the potential to introduce error (Liu et al. 2011), the strong correlation of the
242 regression ($R^2 = 0.86$) (Supp. Fig. 1) suggests that our retrodeformation technique is suitable
243 for the spatial scale of the mapped E Surface. The orientation measurements are different for
244 *Fractofusus* because unlike the frondose organisms there is no differentiation between the top
245 and bottom half of the organism, such as a disc. As such, the angles are limited to a 180 °
246 range of 150 ° to 330 ° with the angle of e.g. 200 ° being equivalent to 20 °.

247 *Statistical analyses*

248 For each taxon population we performed four tests in R v4.0.4. To test for non-uniform
249 distributions of orientation data we used the Rao's Spacing Test of Uniformity using the
250 package CircStats v0.2-6 (Agostinelli and Agostinelli 2018), with a *p*-value < 0.05 indicating
251 a non-uniform distribution (Rao 1976). For our data, a significant *p*-value indicates non-
252 random felling of organisms, with some orientations exhibiting a greater abundance than
253 would otherwise be expected from random felling. In order to test for multimodal
254 distributions within angular data we used the Hermans-Rasson test (HR test of Landler et al.
255 2019) using the package CircMLE v3.0.0 (Fitak and Johnsen 2017). Where multi-modal

256 distributions were found, the mean values for each peak were identified utilising the gaussian
257 finite mixture model-based clustering algorithms of mclust v5.4.7 (Fraley and Raftery 2017).
258 To account for the circular nature of angular data, the density distribution was inspected and
259 split at a minimum to ensure any peaks coincident with 0 ° were not bisected. This split
260 produced a continuous 360 ° density distribution with no assumed peak bisection. When
261 more than one distribution was present (i.e. bidirectional distributions), the data were
262 partitioned into two peaks, whilst unimodal distributions (including those found to be
263 composed of multiple coincident distributions) were left unpartitioned. The circular
264 equivalent to a normal distribution is the von Mises distribution, tested using a Watson's
265 goodness of fit (Agostinelli and Agostinelli 2018). A statistically significant *p*-value output
266 corroborates a von Mises distribution – where a significant von Mises distribution was found,
267 the models of Schnute and Groot (1992) were employed to test for a variety of modelled
268 orientation scenarios. For bimodally-distributed taxa, the constituent distributions were
269 partitioned and frond lengths cross-compared utilising a Mann-Whitney test. Statistical
270 significance would suggest non-uniform sampling from the same parent population; in
271 essence, the orientation-partitioned data would exhibit different frond length distributions.

272 In order to investigate the spatial distribution of populations which exhibited significant
273 multi-modal orientations, random labelling analyses (RLA) were used. RLA are a type of
274 spatial point process analysis whereby the position of each point (here fossil specimen) is
275 kept constant, but the label (here the orientation group) is randomly permutated about the
276 points (Illian et al. 2008). As such, RLAs do not directly measure the aggregation or
277 segregation between labels (here orientation patterns), so do not test the processes that
278 resulted in labels, but instead measure the differences in spatial distributions of the labels
279 independently of the positions of the fossil specimens (cf. Mitchell et al. 2018). Spatial
280 distributions are commonly described using pair correlation functions (PCFs) which describe

how the density of points (i.e. fossil specimens) changes as a function of distance from the average specimen (e.g. Illian et al. 2008). RLAs assess the differences between two characters (orientation group 1 or group 2) of the populations by calculating variations between PCFs by considering the Difference test and the Quotient test (Wiegand and Moloney 2013). The Difference test is the calculation of the difference the distribution of each group in turn (PCF_{11} is the distribution of group 1 and PCF_{22} the distribution of group 2) i.e. PCF_{11}- PCF_{22}. These differences test the relative aggregation (or segregation) of the spatial distributions of the orientations compared to each other. If PCF_{11} - PCF_{22} = 1 then the orientation groups are randomly distributed about the surface. The Quotient test calculates how the relative group (Diggle et al. 2005) changed with respect to the total density (i.e. the joined distribution of both group 1 and group 2). The distribution of group 1 relative to the joined groups $PCF_{1,1+2}$, and group 2 relative to the joined groups $PCF_{2,2+1}$ with the Quotient test as the calculation: $PCF_{1,1+2}$ - $PCF_{21}/PCF_{2,2+1}$. If $PCF_{12}/PCF_{1,1+2}$ - $PCF_{21}/PCF_{2,2+1} > 0$ then group 2 is mainly located in areas with high density of the joint pattern, and group 1 is in low density areas (i.e., group 2 has more neighbours than group 1. If this Quotient is significantly non-zero, then the process underlying the characters is density-dependent. In order to test whether any observed patterns were significantly different from a random distribution we follow Mitchell and Harris 2020 and use two different methods, which are commonly used to establish acceptance or rejection of the null hypotheses for ecological data (e.g. Illian et al. 2008 and references therein): 1) Monte Carlo simulations, and 2) Diggle's goodness-of-fit test p_d, which represents the total squared deviation between the observed pattern and the simulated pattern across the studied distances (Diggle et al. 2005). For each RLA test performed, 999 Monte Carlo simulations were used to generate simulation envelopes around the random PCF difference (e.g. PCF_{11} - PCF_{22} = 0) and the p_d values were calculated using Diggle's goodness-of-fit test. If the observed test (either Difference or

306 Quotient) fell outside the RLA generated Monte Carlo envelopes and also had $p_d < 0.1$, then
307 the distributions were found to be significantly different. RLAs were performed in
308 Programita (Wiegand and Moloney 2013).

309 **RESULTS**

310 For all morphogroups, we found statistically significant non-random distributions using the
311 Rao's Spacing Test of Uniformity and the improved Hermans-Rasson – (all $p < 0.01$, Table
312 1). The majority of taxa exhibited a non-von Mises (i.e. non-normal) distributions as per the
313 Watson's test (Table 1). One *Bradgatia* cohort ($p < 0.05$), and the *Primocandelabrum* stems
314 ($p < 0.01$), and fronds ($p < 0.05$) exhibited von-Mises distributions (Table 1). The von-Mises
315 distributions for *Primocandelabrum* enabled model fitting to the orientation distributions of
316 *Primocandelabrum*, which were found to exhibit bi-modal distributions (Supp. Fig. 2).

317 Analyses of the number of cohorts within each morphogroup orientation distribution varied
318 between 1 and 5 (Table 2, Figure 4). For *C. procerus* and *Plumeropriscum*, the stems and
319 fronds exhibited uni-modal distributions, with similar mean orientations of 195° and 192 ° for
320 *C. procerus* stems and fronds and 178 ° and 177 ° for *Plumeropriscum* (Table 2, Figure 4).
321 The majority (96.77%) of *C. spinosus* stems and fronds exhibited a unimodal distribution
322 (190 ° and 183 ° respectively), with a single outlier orientated at 326 ° for stem and 328 ° for
323 frond (Table 2, Figure 4, Supp. Fig. 3). Similarly, *Primocandelabrum* specimens exhibit a
324 unimodal distribution for their fronds (95.74%, 187 °) and with a minor bimodal component
325 for the stems (89.36%, 183 °; 6.38%, 237 °), with two singleton outliers, and frond at 14 ° and
326 the second with its stem at 119 ° and frond at 98 ° (Table 2, Figure 4, Supp. Fig. 3).
327 *Thectardis* and *Bradgatia* exhibited bi-modal distributions, with different distributions
328 indicated by the mean orientations being notably different between the two groups, in
329 contrast to *Primocandelabrum* and *C. spinosus* (Table 2, Figure 4). The majority of

Bradgatia specimens (57.69%) formed a cohort with the mean orientation of 15 º, with the remainder (42.31%) within the cohort at 188 º (Table 2, Figure 4). The majority of *Thectardis* specimens (74.07%) formed a cohort with the mean orientation of 199 º, with the remainder (25.93%) within the cohort at 17 º (Table 2, Figure 4). The distribution of sampled *Beothukis* specimens formed 5 distinct cohorts (Table 2), with one specimen notably different at 95 º to the other four cohorts, which had similar mean orientations with the unimodal taxa orientations. The small number of specimens within the *Beothukis* distributions indicates that the relatively high number of cohorts could be an artefact of small sample sizes. *Fractofusus* exhibited a multi-modal distribution, with four cohorts at 172 º, 236 º, 295 º and 318 º (Table 2, Figure 4).

Inspection of the distributions in Figure 4 shows that while the number of statistically significant cohorts within each morphogroup varies, the stemmed taxa (*C. spinosus*, *C. procerus*, *Plumeropriscum* and *Primocandelabrum*) and *Beothukis* were all orientated in similar directions, while *Bradgatia* and *Thectardis* had a significant proportion of specimens with an antipodal orientation (Table 2, Figure 4). While the mean orientations of the multiple *Beothukis* cohorts were all tightly clustered, showing clear directionality in a single direction, the *Fractofusus* mean orientations were evenly distributed across the range, with no such directionality (Fig. 4).

Analyses of the bimodally distributed taxa found no significant differences mean frond length for *Bradgatia* (p = 0.1850), or cone length for *Thectardis* (p = 0. 4547) between cohorts. *Bradgatia* was the only taxon that exhibited significant bidirectionality in numbers sufficient for RLA (Fig. 5a). The Quotient test RLA, which describes the relative density dependence of different factors within a spatial population found that there was no density dependence between the two *Bradgatia* orientation groups (p_d = 0.8040, Fig. 5b). The Difference test RLA which tests for the difference between the spatial distributions of the two orientation

355 groups were not significantly different (p_d = 0.4104, Fig 3c.), although the observed
356 difference was close to the outside the simulation envelope which could indicate a larger
357 spatial scale pattern not captured within out data.

358 **DISCUSSION**

359 The orientation distributions of fossil specimens are well established as a mechanism to
360 indicate palaeocurrent directions (Toots 1965; Jones and Dennison 1970). The orientation
361 distribution of a given taxon depends on its mode of life, with erect benthic organisms
362 exhibiting strong directionality, in contrast to non-erect organisms which have limited
363 directionality (Toots 1965; Jones and Dennison 1970; Smith 1980; Demko 1995). These
364 explanations of orientation distributions have been used to understand the mode-of-life of
365 Ediacaran taxa, with qualitative examination of 578 *Fractofusus* specimens showing even
366 orientation distribution suggestive of a reclining mode of life (Gehling and Narbonne 2007).
367 In contrast, Ediacaran fronds such as *Charniodiscus* and *Charnia* have been interpreted as
368 erect organisms, due to the morphological similarities to extant benthos such as sea pens
369 (Seilacher 1992; Laflamme and Narbonne 2008; Laflamme et al. 2012) and - crucially - the
370 orientation of these fronds are noted to have a strongly preferred orientation, suggested to be
371 aligned to the contour-parallel current which felled them (Wood et al. 2003; Narbonne 2005;
372 Laflamme et al. 2012). Strongly orientated organisms have been interpreted as erect because
373 an organism attached to the seafloor at a single point will have the majority of its body pulled
374 by the current, orientating it with its long axis parallel to this current. In contrast, if an
375 organism is reclining on the substrate, it will not be subject to such currents, so will not
376 display strong orientations (Gehling and Narbonne 2007; Mitchell et al. 2015).

377 The relationship between fossil orientation and mode-of-life is pertinent because there has
378 recently been revived debate surrounding the nature of the life habit of the Ediacaran

379 rangeomorphs (e.g. McIlroy et al. 2021). Where fronds have historically been interpreted as
380 displaying a mixture of upright and recumbent lifestyles, recent work has posited that
381 recumbent lifestyles are more likely for some rangeomorph fronds. Orientation analyses
382 allows us to test between these two different life habits in a statistically valid way. This study
383 is the first to quantitatively test the orientation distributions of E surface taxa, and the first to
384 record differences in orientations between the stems and fronds of these taxa. We find
385 significant differences in felling behaviour between the stemless *Bradgatia* and *Thectardis*,
386 *Fractofusus,* and all other taxa (*Beothukis*, the arboreomorphs, *Primocandelabrum*, and
387 *Plumeropriscum*), which show unidirectional felling all oriented towards the south.
388 *Fractofusus* shows no notable directionality in any direction, whereas orientation
389 distributions of *Bradgatia* and *Thectardis* both exhibit evidence of bidirectional felling. We
390 found no height/sized-based correlations with orientation or outliers. Our results confirm the
391 qualitative results of previous authors (Laflamme et al. 2012, Wood et al. 2003; Narbonne et
392 al. 2005; Gehling and Narbonne 2007) whereby frondose taxa such as *Beothukis*,
393 *Charniodiscus* and *Primocandelabrum* were erect in the water-column, anchored to the sea-
394 floor, while *Fractofusus* lived close to the substrate in a reclined habit. Our results do not
395 support recent suggestions that the fronds like *Beothukis* reclined on the sediment in life
396 (McIlroy et al. 2021). The orientation distributions we find for *Bradgatia* and *Thectardis* are
397 also consistent with an upright mode of life and felling in a (bidirectional) current. All of our
398 results and interpretations are based on the behaviour of the majority of specimens within a
399 taxon, and confirm the utility of populations of specimens rather than outliers to infer the
400 ecology for the entire population of a given taxon (e.g. Benhadi-Marín 2018). Describing
401 population distributions enables intra-specific variability to be captured, and thus enables
402 comparison between populations. Indeed, it is not possible to compare the orientations of two
403 specimens in a statistically rigorous and robust way without accounting for intra-specific

variability, i.e. without quantifying the population behaviour. There are, notably, multiple cohorts within the orientation distributions of *Beothukis*. However, while *C. procerus*, for example, exhibits different mean orientation directionality to *Beothukis*, the 95% confidence interval (as given by two sigma) places all bar one specimen of *Beothukis* (the holotype, oriented at 95 º) the *C. procerus* confidence interval – and indeed, within the 95% confidence intervals of all other southerly-oriented taxa. Thus, the *Beothukis* and *C. procerus* populations do not have significantly different orientations. It is possible of course that the *Beothukis* holotype belongs to a different species than the remainder of the population assigned by us to that taxon based on branching characters. However, recent work on the taxonomy of *Beothukis*, which demonstrates that the holotype is well within all other specimens with comparable morphology, and which were assigned by those authors to that taxon (Hawco et al. 2020) renders this unlikely. Indeed, an outlier of *Primocandelabrum* – whose morphology, and the orientations of the rest of the population, are entirely at odds with a reclined mode of life – is also oriented at 95 º. Our orientation analyses of the *Beothukis* population demonstrates how the holotype orientation is an outlier and not representative of the population. Our results thus confirm an erect lifestyle for *Beothukis* (Wood et al. 2003; Laflamme and Narbonne 2008; Laflamme et al. 2012), contra McIlroy et al. 2020.

Charniodiscus procerus specimens – the taxon with the proportionally longest stem of any studied here (Laflamme et al. 2004) – are all oriented south, in a single cohort, with 1 outlier individual oriented antipodally (Supp. Fig. 3). All bar one specimen of *Beothukis* is oriented south, although notably with greater variance than the stemmed arboreomorphs (Fig. 4). All *Plumeropriscum* specimens are oriented south, along with the majority of *Primocandelabrum* (Fig. 4). Two *Primocandelabrum* specimens are oriented in a different orientation, away from the main direction (Fig. 4, Supp. Fig. 3). In contrast, *Bradgatia* specimens are divided almost equally between north and south felling directions (Fig. 4). These data would suggest that

there is a correlation between proportional stem length and felling direction, and for the multifoliate taxa, there seems to be a strong correlation between presence of a stem and felling direction. *Thectardis* – with its narrow base and wide top – like *Bradgatia*, also shows a significant portion felled in the northern direction (Fig. 4).

Together, our data suggest that those taxa with bases that are proportionally narrow compared to the widths of their tops (*Thectardis* and *Bradgatia*) show significantly different felling behaviours to those taxa that are more elongate and equal in shape, and that those taxa with the longest and thickest stems show the most consistent felling direction. *Beothukis*, for example, appears to show a sympodial central axis, and has the widest spread of any of the unifoliate and dominantly south-felled taxa. Equally, although *Primocandelabrum* has a sturdy stem, it has a proportionally wide top, and two specimens that are felled at a different angle from the main population. *Charniodiscus spinosus* has a much shorter stem than *C. procerus*, and also has a few specimens that are felled antipodally. The top-heavy morphology of *Primocandelabrum*, *Bradgatia* and *Thectardis* would presumably induce greater drag compared to the more stream-lined unifoliate fronds, making them more susceptible to felling – and also potentially to adhesion to the matground – with the sturdy stems of *Primocandelabrum* helping to redress this susceptibility in all bar a few individual cases.

Random labelling analyses suggest that these differences are not an artifact of different flow regimes in different areas, indicating that differences in orientations between stemmed and stemless organisms may reflect genuine differences in the effect of flow on stemmed and stemless taxa. Fronds and stems behave differently in flow: at a flow velocity of 0 ms^{-1}, both the frond and the stem will be fully upright, with no deflection, but as the flow velocity increases the tubular cross-section of the stem maximises the second moment of area, thus reducing the extent of bending under stress, and so this tubular morphology would serve to

reduce the probability of failure via buckling (Wegst and Ashby 2007). Perhaps, because of this morphology the stem impeded felling of stemmed taxa within the enhanced velocities of the turbulent head of a turbidite, according with studies concerning the mechanical properties of stems, for example crinoids and aquatic plants (Baumiller and Ausich 1996; Ming-Chao and Chang-Feng 1996; Luhar and Nepf 2011).

These data support a two-phase model of felling (Fig. 6), corresponding to the different flow regimes within a gravity flow. We infer that during the turbulent head of the flow, most fronds were buffeted by Kelvin-Helmholtz vortices. However, some easily-felled taxa (*Bradgatia* and *Thectardis*) were felled by this turbulence, producing a bimodal distribution of felling orientations (Figs 4, 6). The transition to laminar flow within the body of the turbidity flow led to the felling of most remaining fronds, in a unimodal distribution (Figs 4, 6). In Charnwood Forest, we know that at least some fronds were capable of surviving small-scale disturbance events (Wilby et al. 2015). Wilby et al. focussed on the bimodal population structures of the unifoliate rangeomorph *Charnia*, but documented other, stemmed taxa that were also preserved with a bimodal population structure (*Primocandelabrum*, *Hylaecullulus* and *Charniodiscus*). Together with our data, this suggests that stemmed and elongate taxa showed greater survivability in high velocity flow. Height in the water column has previously been demonstrated to increase propagule dispersal, and doesn't appear to provide refuge from resource competition (Mitchell and Kenchington 2018). Our work suggests that stems may have had an additional function – lending greater resilience to felling in turbulent and high velocity flow regimes. These insights hint at potential environmental influences on the morphological composition of Ediacaran communities.

CONCLUSIONS

We provide the first quantitative analyses of the orientation of populations of specimens from the Mistaken Point E surface. Our data support traditional palaeobiological models for the life habits of different organisms which lived in this community, with the majority of frondose organisms living upright in the water column while the spindle-shaped *Fractofusus* lived flat on the seafloor. Previous authors have suggested that current type and flow rate may impact community composition, but we demonstrate for the first time how the presence or absence of anatomical features impact survivability in different flow regimes. Specifically, we find that the presence of a stem (and potentially its proportional length) lends greater resilience to turbulent currents. Future work may find that such traits affect the presence and abundance of different morphologies under different environmental conditions, and potentially even the structuring of communities as they experience changing flow conditions.

Acknowledgements – The Parks and Natural Areas Division (PNAD), Department of Environment and Conservation, Government of Newfoundland and Labrador, provided permits to conduct research within the Mistaken Point Ecological Reserve (MPER) in 2010, 2016 and 2017. Readers are advised that access to MPER is by scientific research permit only. This work has been supported by the Natural Environment Research Council Independent Research Fellowship NE/S014756/1 to EGM and a Natural Environment Research Council grant NE/V010859/1 to FSD. FSD acknowledges support from the Royal Commission for the Exhibition of 1851 and Merton College, Oxford. CGK was supported by Leverhulme Trust (ECF-2018-542) and by the Isaac Newton Trust 18.08(H).

Author contributions - PBV conceived and designed the project. Analyses were performed PBV and EGM. PBV, EGM and CGK contributed to data collection from photosquares and all authors contributed to the writing up of the final manuscript.

Supporting information - Supplementary data are available at: (link).

Data accessibility statement - The original data presented here can be accessed through the Supporting Information.

References

Agostinelli, C., and M. C. Agostinelli. 2018: CircStats Package. *in Topics in Circular Statistics*. p.

Baas, J. H., and J. L. Best. 2002: Turbulence Modulation in Clay-Rich Sediment-Laden Flows and Some Implications for Sediment Deposition. Journal of Sedimentary Research 72:336–340.

Baas, J. H., J. L. Best, J. Peakall, and M. Wang. 2009: A Phase Diagram for Turbulent, Transitional, and Laminar Clay Suspension Flows. Journal of Sedimentary Research 79:162–183.

Bamforth, E. L., and G. M. Narbonne. 2009: New ediacaran rangeomorphs from Mistaken Point, Newfoundland, Canada. Journal of Paleontology 83:897–913.

Bamforth, E. L., G. M. Narbonne, and M. M. Anderson. 2008: Growth and ecology of a multi-branched Ediacaran rangeomorph from the Mistaken Point assemblage, Newfoundland. Journal of Paleontology 82:763–777.

Baumiller, T. K., and W. I. Ausich. 1996: Crinoid stalk flexibility: theoretical predictions and fossil stalk postures. Lethaia 29:47–59.

Benhadi-Marín, J. 2018: A conceptual framework to deal with outliers in ecology. Biodiversity and Conservation 27:3295–3300.

Bobrovskiy, I., J. M. Hope, A. Ivantsov, B. J. Nettersheim, C. Hallmann, and J. J. Brocks. 2018: Ancient steroids establish the Ediacaran fossil Dickinsonia as one of the earliest animals. Science 361:1246–1249.

524 Boynton, H., and T. D. Ford. 1995: Ediacaran Fossils from the Precambrian (Charnian
525 Supergroup) of Charnwood Forest, Leicestershire, England. Mercian Geologist
526 13:165–182.
527 Brasier, M. D., and J. B. Antcliffe. 2009: Evolutionary relationships within the Avalonian
528 Ediacara biota: new insights from laser analysis. Journal of the Geological Society
529 166:363–384.
530 Budd, G. E., and S. Jensen. 2017: The origin of the animals and a 'Savannah' hypothesis for
531 early bilaterian evolution. Biological Reviews 92:446–473.
532 Cantero, M. I., A. Cantelli, C. Pirmez, S. Balachandar, D. Mohrig, T. A. Hickson, T. Yeh, H.
533 Naruse, and G. Parker. 2012: Emplacement of massive turbidites linked to extinction
534 of turbulence in turbidity currents. Nature Geoscience 5:42–45.
535 Cartigny, M. J. B., J. T. Eggenhuisen, E. W. M. Hansen, and G. Postma. 2013:
536 Concentration-Dependent Flow Stratification In Experimental High-Density Turbidity
537 Currents and Their Relevance To Turbidite Facies Models. Journal of Sedimentary
538 Research 83:1047–1065.
539 Clapham, M. E., G. M. Narbonne, and J. G. Gehling. 2003: Paleoecology of the oldest known
540 animal communities: Ediacaran assemblages at Mistaken Point, Newfoundland.
541 Paleobiology 29:527–544.
542 Clapham, M. E., G. M. Narbonne, J. G. Gehling, C. Greentree, and M. M. Anderson. 2004:
543 Thectardis avalonensis: A new Ediacaran fossil from the Mistaken Point biota,
544 Newfoundland. Journal of Paleontology 78:1031–1036.
545 Cuthill, J. F. H., and S. C. Morris. 2014: Fractal branching organizations of Ediacaran
546 rangeomorph fronds reveal a lost Proterozoic body plan. Proceedings of the National
547 Academy of Sciences 111:13122–13126.

548 Cuthill, J. F. H., and J. Han. 2018: Cambrian petalonamid Stromatoveris phylogenetically
549 links Ediacaran biota to later animals. Palaeontology 61:813–823.
550 Dececchi, T. A., G. M. Narbonne, C. Greentree, and M. Laflamme. 2017: Relating Ediacaran
551 Fronds. Paleobiology 43:171–180.
552 Demko, T. 1995: Proceedings of the Third Annual Fossils of Arizona Symposium, November
553 18, 1995. *in* M. S. Museum, ed. American Traveler Press, p.
554 Diggle, P., P. Zheng, and P. Durr. 2005: Nonparametric estimation of spatial segregation in a
555 multivariate point process: bovine tuberculosis in Cornwall, UK. Journal of the Royal
556 Statistical Society: Series C (Applied Statistics) 54:645–658.
557 Dunn, F. S., A. G. Liu, and P. C. J. Donoghue. 2018: Ediacaran developmental biology.
558 Biological Reviews 93:914–932.
559 Dunn, F. S., P. R. Wilby, C. G. Kenchington, D. V. Grazhdankin, P. C. J. Donoghue, and A.
560 G. Liu. 2019: Anatomy of the Ediacaran rangeomorph Charnia masoni. Papers in
561 Palaeontology 5:157–176.
562 Dunn, F. S., A. G. Liu, D. V. Grazhdankin, P. Vixseboxse, J. Flannery-Sutherland, E. Green,
563 S. Harris, P. R. Wilby, and P. C. J. Donoghue. 2021: The developmental biology of
564 Charnia and the eumetazoan affinity of the Ediacaran rangeomorphs. Science
565 Advances 7:eabe0291.
566 Dynowski, J. F., J. H. Nebelsick, A. Klein, and A. Roth-Nebelsick. 2016: Computational
567 Fluid Dynamics Analysis of the Fossil Crinoid Encrinus liliiformis (Echinodermata:
568 Crinoidea). PLOS ONE 11:e0156408.
569 Fitak, R. R., and S. Johnsen. 2017: Bringing the analysis of animal orientation data full circle:
570 model-based approaches with maximum likelihood. Journal of Experimental Biology
571 220:3878–3882.

572 Flude, L. I., and G. M. Narbonne. 2008: Taphonomy and ontogeny of a multibranched
573 Ediacaran fossil: Bradgatia from the Avalon Peninsula of Newfoundland. Canadian
574 Journal of Earth Sciences 45:1095–1109.
575 Fraley, C., and A. E. Raftery. 2017: MCLUST Version 3 for R: Normal Mixture Modeling
576 and Model-Based Clustering∗. :57.
577 Gehling, J. G., and G. M. Narbonne. 2007: Spindle-shaped Ediacara fossils from the
578 Mistaken Point assemblage, Avalon Zone, Newfoundland. Canadian Journal of Earth
579 Sciences 44:367–387.
580 Ghisalberti, M., D. A. Gold, M. Laflamme, M. E. Clapham, G. M. Narbonne, R. E.
581 Summons, D. T. Johnston, and D. K. Jacobs. 2014: Canopy Flow Analysis Reveals
582 the Advantage of Size in the Oldest Communities of Multicellular Eukaryotes.
583 Current Biology 24:305–309.
584 Hallworth, M. A., J. C. Phillips, H. E. Huppert, and R. S. J. Sparks. 1993: Entrainment in
585 turbulent gravity currents. Nature 362:829–831.
586 Haughton, P., C. Davis, W. McCaffrey, and S. Barker. 2009: Hybrid sediment gravity flow
587 deposits – Classification, origin and significance. Marine and Petroleum Geology
588 26:1900–1918.
589 Hawco, J. B., C. G. Kenchington, R. S. Taylor, and D. McIlory. 2020: A MULTIVARIATE
590 STATISTICAL ANALYSIS OF THE EDIACARAN RANGEOMORPH TAXA
591 BEOTHUKIS AND CULMOFRONS. PALAIOS 35:495–511.
592 Hofmann, H. J., S. J. O'Brien, and A. F. King. 2008: Ediacaran biota on Bonavista Peninsula,
593 Newfoundland, Canada. Journal of Paleontology 82:1–36.
594 Ichaso, A. A., R. W. Dalrymple, and G. M. Narbonne. 2007: Paleoenvironmental and basin
595 analysis of the late Neoproterozoic (Ediacaran) upper Conception and St. John's

596 groups, west Conception Bay, Newfoundland. Canadian Journal of Earth Sciences
597 44:25–41.
598 Illian, J., P. A. Penttinen, D. H. Stoyan, and D. D. Stoyan. 2008: Statistical Analysis and
599 Modelling of Spatial Point Patterns. Wiley, p.
600 Jones, M. L., and J. M. Dennison. 1970: Oriented fossils as paleocurrent indicators in
601 Paleozoic lutites of southern Appalachians. Journal of Sedimentary Research 40:642–
602 649.
603 Kenchington, C. G., and P. R. Wilby. 2017: Rangeomorph classification schemes and intra-
604 specific variation: are all characters created equal? Geological Society, London,
605 Special Publications 448:221–250.
606 Kenchington, C. G., S. J. Harris, P. B. Vixseboxse, C. Pickup, and P. R. Wilby. 2018: The
607 Ediacaran fossils of Charnwood Forest: Shining new light on a major biological
608 revolution. Proceedings of the Geologists' Association 129:264–277.
609 Kiipli, T., E. Kiipli, T. Kallaste, R. Hints, P. Somelar, and K. Kirsimäe. 2007: Altered
610 volcanic ash as an indicator of marine environment, reflecting ph and sedimentation
611 rate – example from the Ordovician Kinnekulle bed of Baltoscandia. Clays and Clay
612 Minerals 55:177–188.
613 Koehl, M. A. R. 1977a: Effects of Sea Anemones on the Flow Forces They Encounter.
614 Journal of Experimental Biology 69:87–105.
615 ———. 1977b: Mechanical Organization of Cantileverlike Sessile Organisms: Sea
616 Anemones. Journal of Experimental Biology 69:127–142.
617 Laflamme, M., and G. M. Narbonne. 2008: Ediacaran fronds. Palaeogeography,
618 Palaeoclimatology, Palaeoecology 258:162–179.

619 Laflamme, M., G. M. Narbonne, and M. M. Anderson. 2004: Morphometric analysis of the
620 Ediacaran frond Charniodiscus from the Mistaken Point Formation, Newfoundland.
621 Journal of Paleontology 78:827–837.
622 Laflamme, M., S. Xiao, and M. Kowalewski. 2009: Osmotrophy in modular Ediacara
623 organisms. Proceedings of the National Academy of Sciences 106:14438–14443.
624 Laflamme, M., L. I. Flude, and G. M. Narbonne. 2012: Ecological tiering and the evolution
625 of a stem: the oldest stemmed frond from the Ediacaran of Newfoundland, Canada.
626 Journal of Paleontology 86:193–200.
627 Laflamme, M., J. G. Gehling, and M. L. Droser. 2018: Deconstructing an Ediacaran frond:
628 three-dimensional preservation of Arborea from Ediacara, South Australia. Journal of
629 Paleontology 92:323–335.
630 Landler, L., G. D. Ruxton, and E. P. Malkemper. 2019: The Hermans–Rasson test as a
631 powerful alternative to the Rayleigh test for circular statistics in biology. BMC
632 Ecology 19:30.
633 Liu, A. G., C. G. Kenchington, and E. G. Mitchell. 2015: Remarkable insights into the
634 paleoecology of the Avalonian Ediacaran macrobiota. Gondwana Research 27:1355–
635 1380.
636 Liu, A. G., D. Mcilroy, J. B. Antcliffe, and M. D. Brasier. 2011: Effaced preservation in the
637 Ediacara biota and its implications for the early macrofossil record. Palaeontology
638 54:607–630.
639 Liu, X., and Y. Jiang. 2014: Direct numerical simulations of boundary condition effects on
640 the propagation of density current in wall-bounded and open channels. Environmental
641 Fluid Mechanics 14:387–407.
642 Luhar, M., and H. M. Nepf. 2011: Flow-induced reconfiguration of buoyant and flexible
643 aquatic vegetation. Limnology and Oceanography 56:2003–2017.

644 Mason, S. J., and G. M. Narbonne. 2016: Two new Ediacaran small fronds from Mistaken
645 Point, Newfoundland. Journal of Paleontology 90:183–194.
646 Matthews, J. J., A. G. Liu, C. Yang, D. McIlroy, B. Levell, and D. J. Condon. 2021: A
647 Chronostratigraphic Framework for the Rise of the Ediacaran Macrobiota: New
648 Constraints from Mistaken Point Ecological Reserve, Newfoundland. GSA Bulletin.
649 McIlroy, D., J. Hawco, C. McKean, R. Nicholls, G. Pasinetti, and R. Taylor. 2021:
650 Palaeobiology of the reclining rangeomorph Beothukis from the Ediacaran Mistaken
651 Point Formation of southeastern Newfoundland. Geological Magazine:1–15.
652 Ming-Chao, L., and D. Chang-Feng. 1996: Drag, morphology and mechanical properties of
653 three species of octocorals. Journal of Experimental Marine Biology and Ecology 1–
654 2:13–22.
655 Mitchell, E. G., and C. G. Kenchington. 2018: The utility of height for the Ediacaran
656 organisms of Mistaken Point. Nature Ecology & Evolution 2:1218–1222.
657 Mitchell, E. G., and N. J. Butterfield. 2018: Spatial analyses of Ediacaran communities at
658 Mistaken Point. Paleobiology 44:40–57.
659 Mitchell, E. G., and S. Harris. 2020: Mortality, Population and Community Dynamics of the
660 Glass Sponge Dominated Community “The Forest of the Weird” From the Ridge
661 Seamount, Johnston Atoll, Pacific Ocean. Frontiers in Marine Science 7.
662 Mitchell, E. G., C. G. Kenchington, S. Harris, and P. R. Wilby. 2018: Revealing
663 rangeomorph species characters using spatial analyses. Canadian Journal of Earth
664 Sciences 55:1262–1270.
665 Mitchell, E. G., C. G. Kenchington, A. G. Liu, J. J. Matthews, and N. J. Butterfield. 2015:
666 Reconstructing the reproductive mode of an Ediacaran macro-organism. Nature
667 524:343–346.

668 Mitchell, E. G., S. Harris, C. G. Kenchington, P. Vixseboxse, L. Roberts, C. Clark, A.
669 Dennis, A. G. Liu, and P. R. Wilby. 2019: The importance of neutral over niche
670 processes in structuring Ediacaran early animal communities. Ecology Letters
671 22:2028–2038.
672 Mitchell, E. G., N. Bobkov, N. Bykova, A. Dhungana, A. Kolesnikov, I. R. P. Hogarth, A. G.
673 Liu, T. M. R. Mustill, N. Sozonov, S. Xiao, and D. V. Grazhdankin. 2020: The
674 influence of environmental setting on the community ecology of Ediacaran
675 organisms. Interface Focus 10.
676 Narbonne, G. M. 2004: Modular Construction of Early Ediacaran Complex Life Forms.
677 Science 305:1141–1144.
678 ———. 2005: THE EDIACARA BIOTA: Neoproterozoic Origin of Animals and Their
679 Ecosystems. Annual Review of Earth and Planetary Sciences 33:421–442.
680 Narbonne, G. M., and J. G. Gehling. 2003: Life after snowball: The oldest complex
681 Ediacaran fossils. Geology 31:27–30.
682 Noble, S. R., D. J. Condon, J. N. Carney, P. R. Wilby, T. C. Pharaoh, and T. D. Ford. 2015:
683 U-Pb geochronology and global context of the Charnian Supergroup, UK: Constraints
684 on the age of key Ediacaran fossil assemblages. GSA Bulletin 127:250–265.
685 Rao, J. S. 1976: Some Tests Based on Arc-Lengths for the Circle. Sankhyā: The Indian
686 Journal of Statistics, Series B (1960-2002) 38:329–338.
687 Schnute, J. T., and K. Groot. 1992: Statistical analysis of animal orientation data. Animal
688 Behaviour 43:15–33.
689 Seilacher, A. 1992: Vendobionta and Psammocorallia: lost constructions of Precambrian
690 evolution. Journal of the Geological Society 149:607–613.
691 Shen, B., L. Dong, S. Xiao, and M. Kowalewski. 2008: The Avalon Explosion: Evolution of
692 Ediacara Morphospace. Science 319:81–84.

693 Smith, P. L. 1980: Determining the in situ Orientation of Fossil Bilateral Symmetry Planes
694 during Paleocurrent Analysis. Journal of Paleontology 54:1121–1123.
695 Sparks, R. S. J., and C. J. N. Wilson. 1983: Flow-head deposits in ash turbidites. Geology
696 11:348–351.
697 Sperling, E. A., K. J. Peterson, and M. Laflamme. 2011: Rangeomorphs, Thectardis
698 (Porifera?) and dissolved organic carbon in the Ediacaran oceans. Geobiology 9:24–
699 33.
700 Talling, P. J., D. G. Masson, E. J. Sumner, and G. Malgesini. 2012: Subaqueous sediment
701 density flows: Depositional processes and deposit types. Sedimentology 59:1937–
702 2003.
703 Toots, H. 1965: Orientation and Distribution of Fossils as Environmental Indicators. :219–
704 229.
705 Waggoner, B. 2003: The Ediacaran Biotas in Space and Time. Integrative and Comparative
706 Biology 43:104–113.
707 Wegst, U. G. K., and M. F. Ashby. 2007: The structural efficiency of orthotropic stalks,
708 stems and tubes. Journal of Materials Science 42:9005–9014.
709 Wiegand, T., and K. A. Moloney. 2013: Handbook of Spatial Point-Pattern Analysis in
710 Ecology. CRC Press, p.
711 Wilby, P. R., C. G. Kenchington, and R. L. Wilby. 2015: Role of low intensity environmental
712 disturbance in structuring the earliest (Ediacaran) macrobenthic tiered communities.
713 Palaeogeography, Palaeoclimatology, Palaeoecology 434:14–27.
714 Wood, D. A., R. W. Dalrymple, G. M. Narbonne, J. G. Gehling, and M. E. Clapham. 2003:
715 Paleoenvironmental analysis of the late Neoproterozoic Mistaken Point and Trepassey
716 formations, southeastern Newfoundland. Canadian Journal of Earth Sciences
717 40:1375–1391.

718 Wood, R., A. G. Liu, F. Bowyer, P. R. Wilby, F. S. Dunn, C. G. Kenchington, J. F. H.
719 Cuthill, E. G. Mitchell, and A. Penny. 2019: Integrated records of environmental
720 change and evolution challenge the Cambrian Explosion. Nature Ecology &
721 Evolution 3:528–538.
722 Xiao, S., and M. Laflamme. 2009: On the eve of animal radiation: phylogeny, ecology and
723 evolution of the Ediacara biota. Trends in Ecology and Evolution 24:31–40.
724

Figure and Table Captions

Figure 1: E surface taxa included in this study. A) *Charniodiscus procerus* and *Beothukis* and B) Close up of *Beothukis* C) *Charniodiscus spinosus* D) *Thectardis*, E) *Fractofusus* and *Plumeropriscum* and F) *Primocandelabrum*. Scale bar is 5cm.

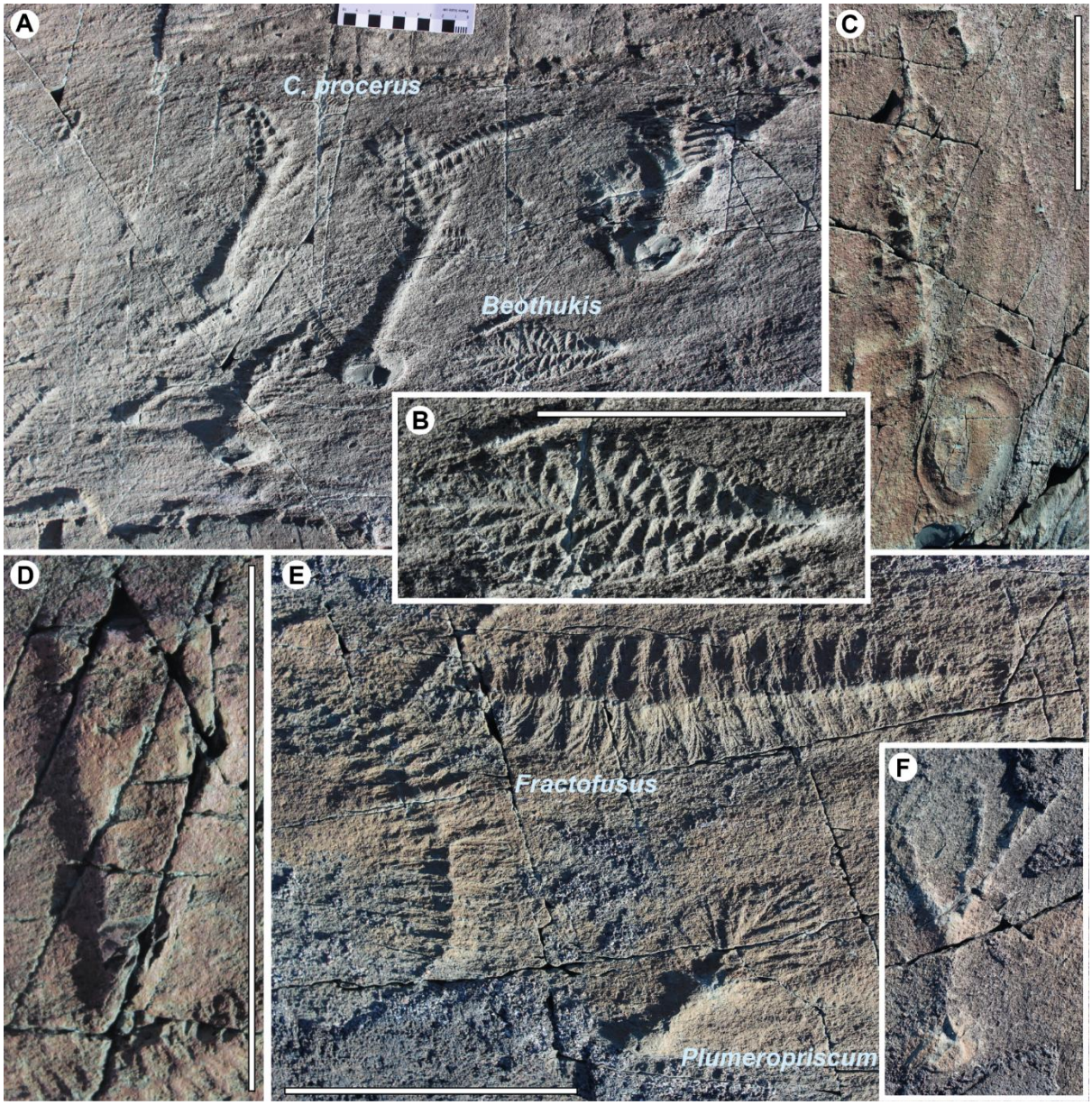

730 **Figure 2:** Geological Map after Liu (2016) and Matthews et al. (2021) showing the location
731 of the E surface, Mistaken Point within Newfoundland, Canada, and the stratigraphy and age
732 from Matthews et al. 2021.

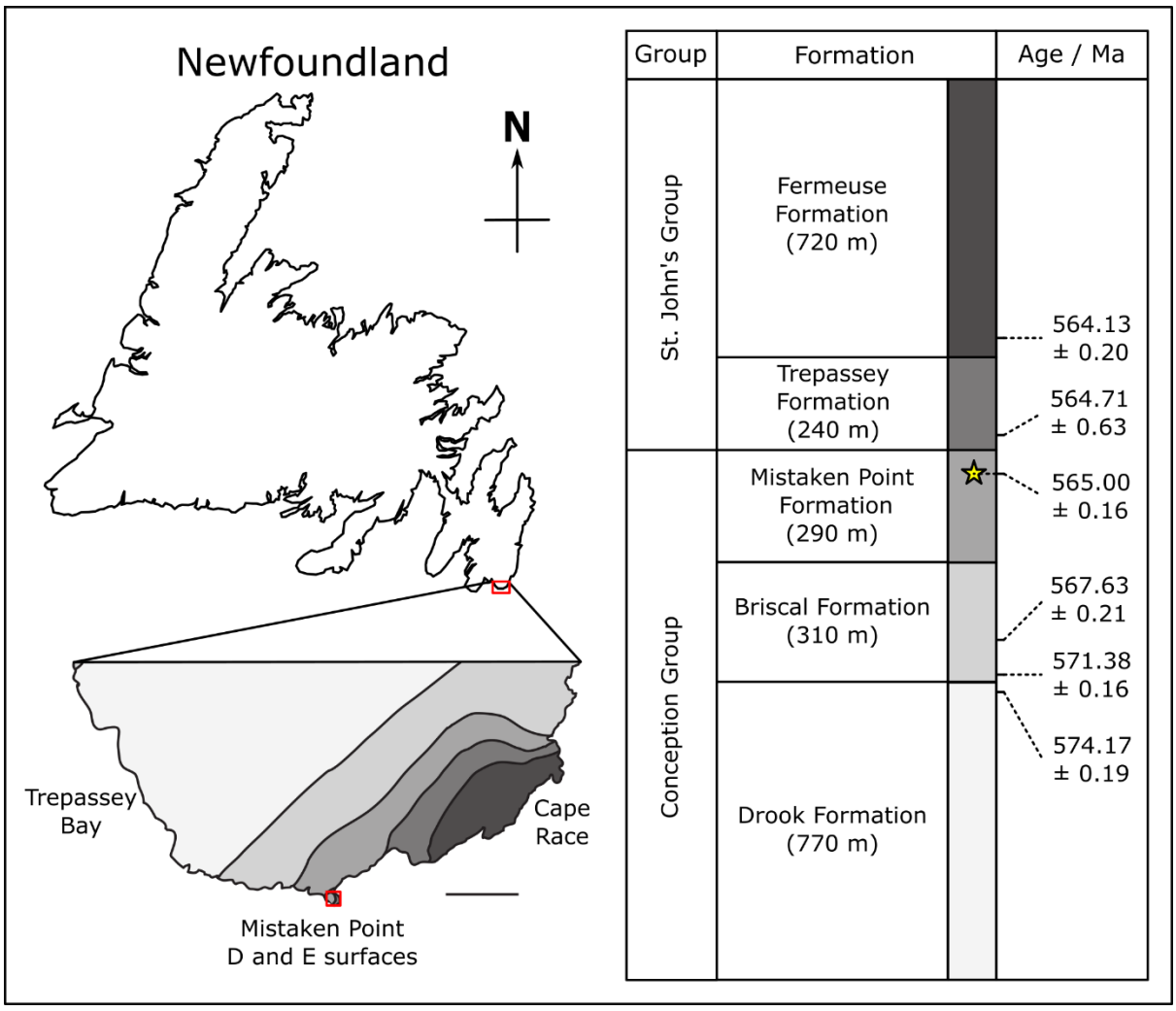

733

734

735 **Figure 3:** Specimen measurements. An example specimen (A) showing the retrodeformation
736 of the disc B to C, and D) the measurements collected for each specimen. The position of the
737 disc is denoted as (x_{disc},y_{disc}); the length of the frond as L_f; the length of the stem as L_s; the
738 angle of the frond as θ_f; and the angle of the stem as θ_s.

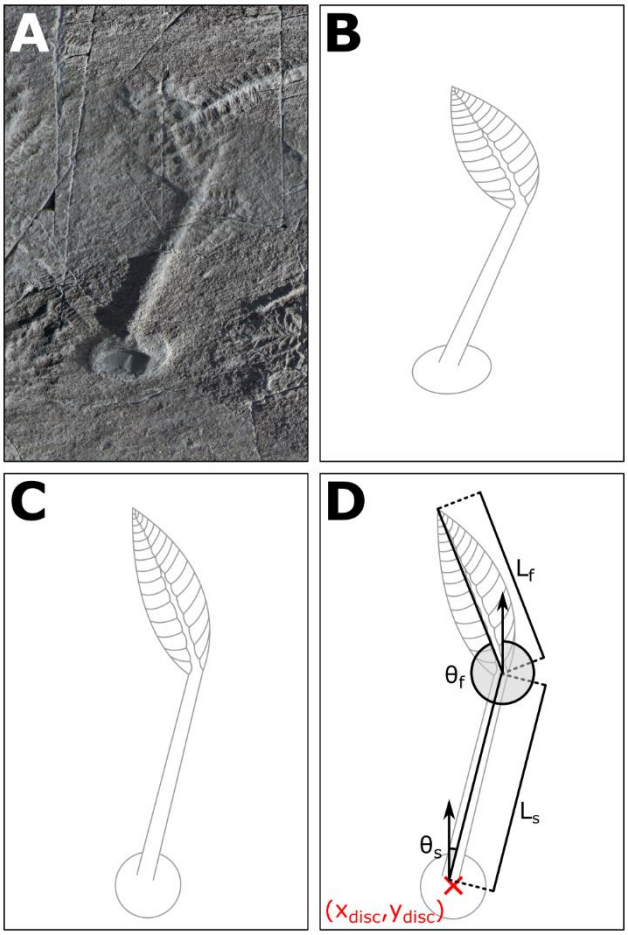

739

740 **Figure 4:** Rose diagrams of the population. Blue indicates frond orientations, Red, the stem
741 orientations and yellow for *Thectardis*. Arrows indicate the mean(s) of the cohort orientation
742 distributions, with starred arrows indicating where outliers have been removed.

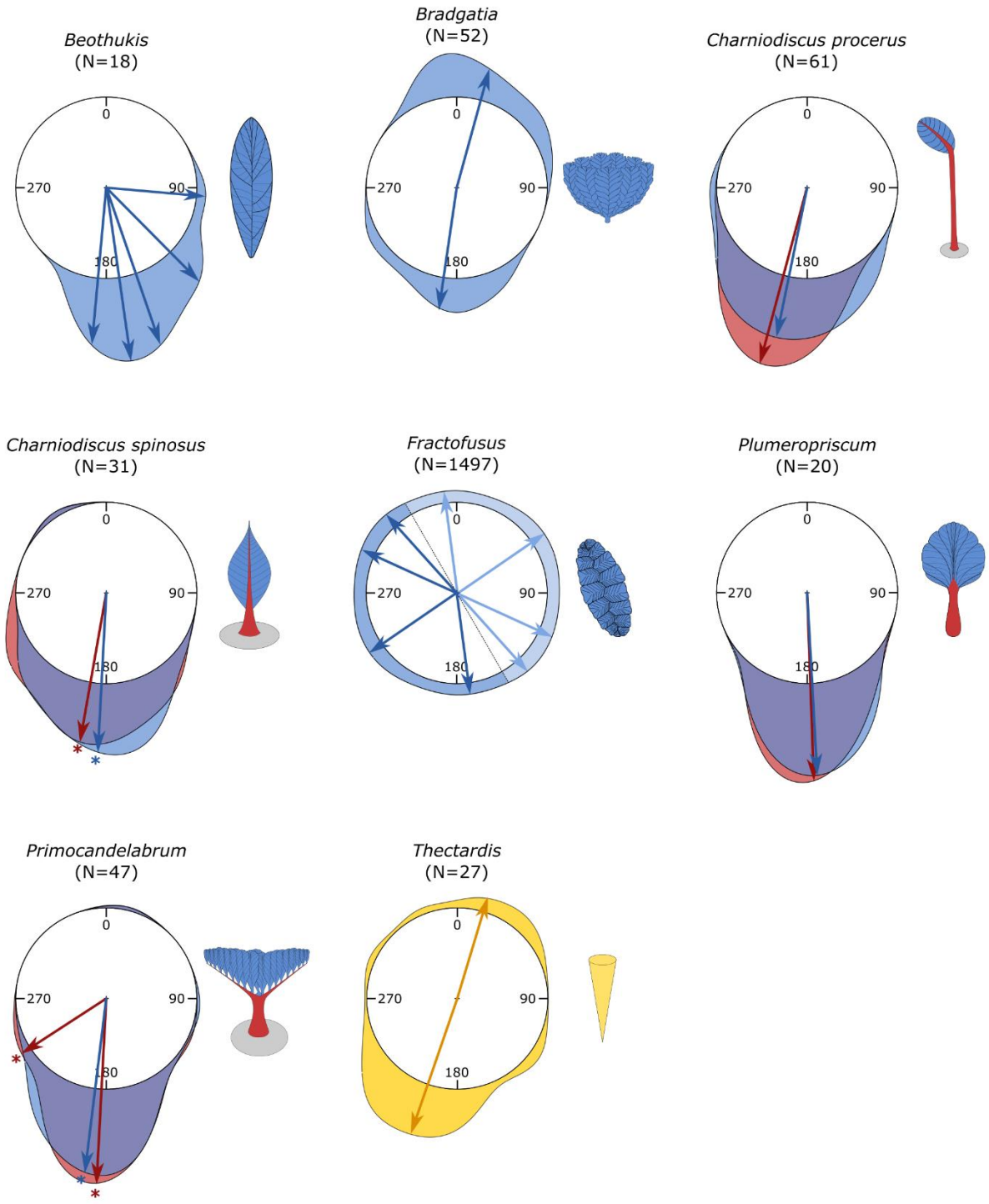

743

744 **Figure 5:** Random labelling analyses for the two cohorts of *Bradgatia.* A) Mapped *Bradgatia*
745 on the E surface, showing the two directions in light and dark blue. The diameter of the
746 circles represents the height of the specimens. Light grey area is the retrodeformed outline of
747 the E surface.

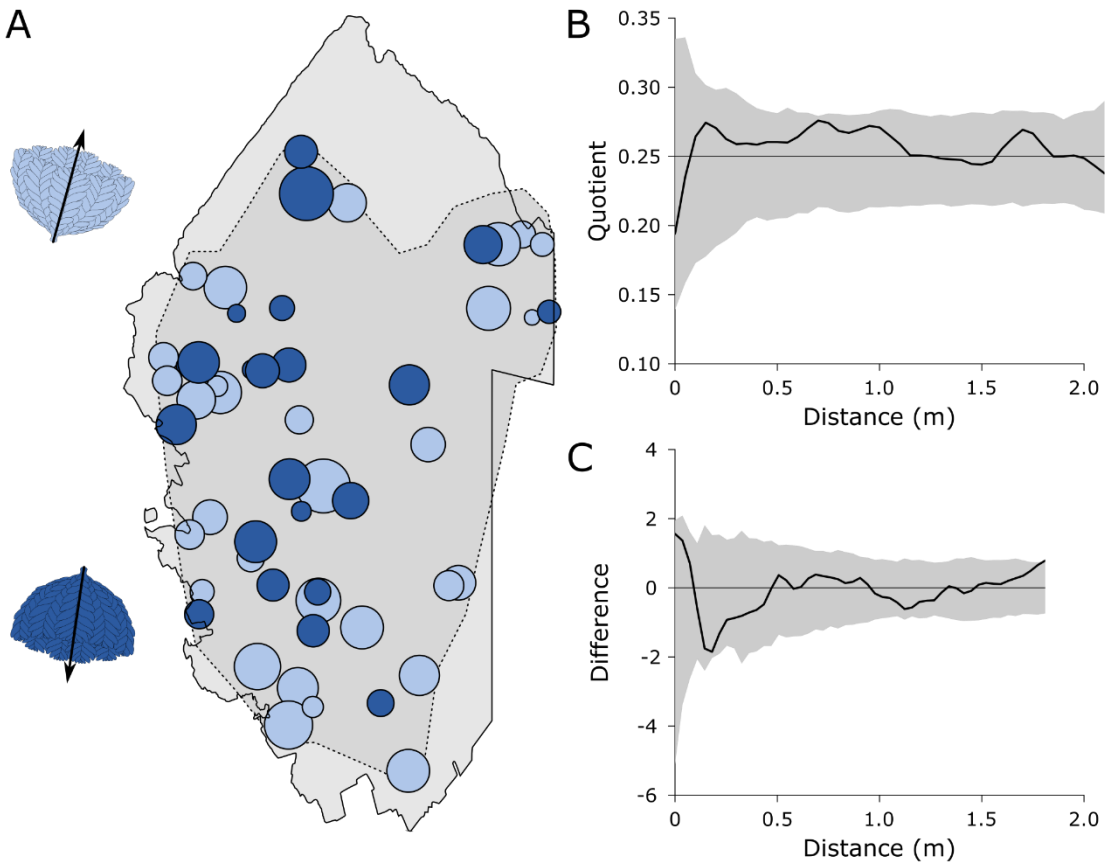

748

749 **Figure 6.** Schematic illustrating the sequence of events that yield the preserved orientation
750 distributions. A) E surface community in life, with all fronds bar *Fractofusus* having an
751 upright mode of life. B) The turbid head of the gravity flow fells organisms with a high centre
752 of gravity, including *Thectardis* and *Bradgatia*, producing a bimodal orientation distribution
753 pattern. C) The laminar tail of the gravity flow fells all other upright fronds on the surface. D)
754 Ash settles out of the flow, and smothers the community with the preserved distribution of
755 orientations. Yellow = *Thectardis*; pink = *Bradgatia*; dark blue = *Fractofusus*; grey =
756 *Charniodiscus procerus* and *Charniodiscus spinosus*; blue = upright fronds felled with a
757 unimodal orientation (*Beothukis*, *Plumeropriscum* and *Primocandelabrum*).

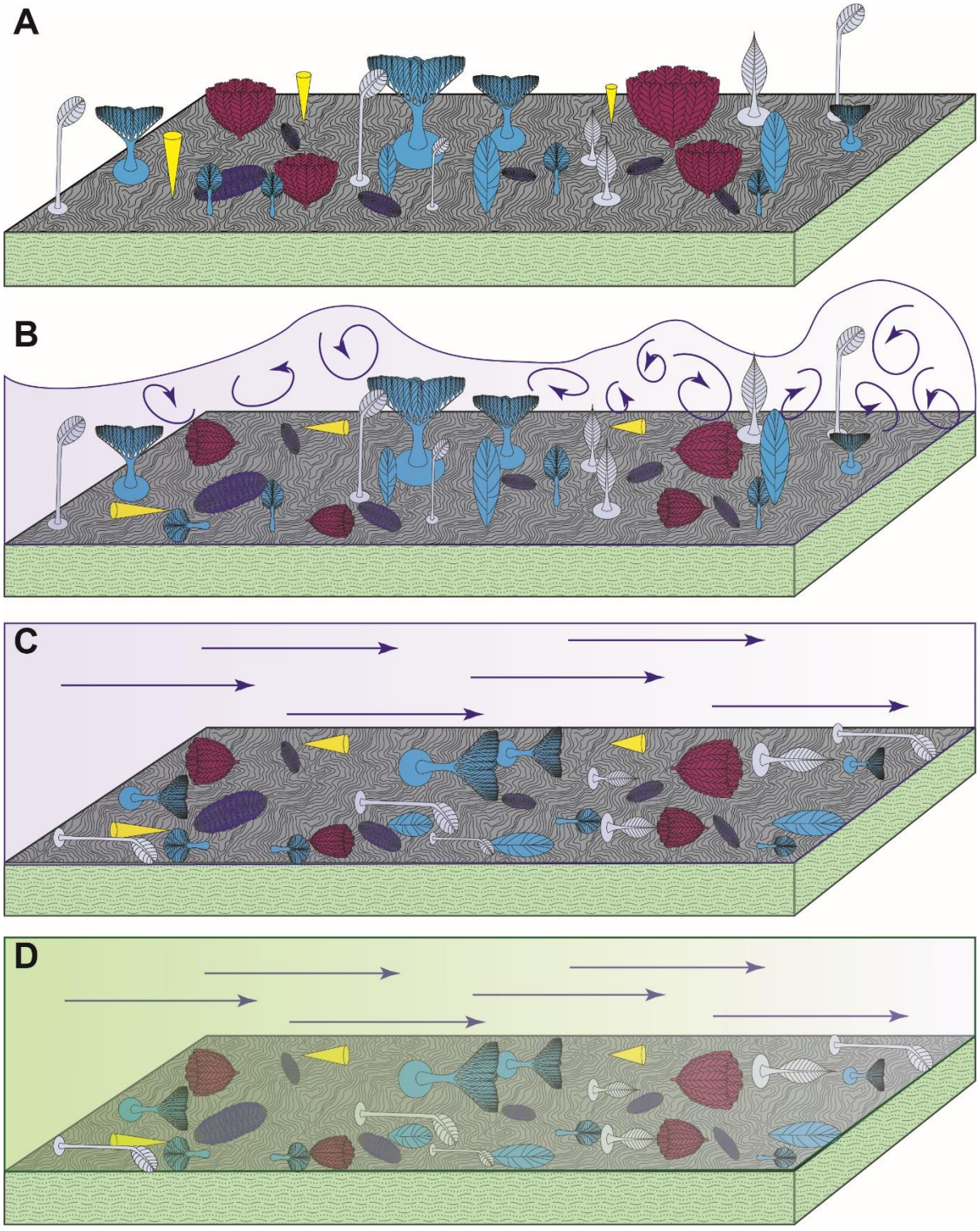

758

759 **Table 1.** Results of uniformity tests, with 5% significance levels used to indicate rejection of
760 the null models i.e. non-random orientations for the Rao's spacing and Hermans-Rasson tests
761 and von Mises distribution (normally distributed orientation data) for the Watson's test.

762

Taxa	**Measurement**	**Rao's Test *p*-value**	**Hermans-Rasson test *p*-value**	**Watson's Test *p*-value**
Beothukis	Fronds	< 0.001	0.0001	> 0.10
Bradgatia	Fronds	< 0.001	0.0001	> 0.10
				< 0.05
C. procerus	Stems	< 0.001	0.0001	> 0.10
	Fronds	< 0.001	0.0001	> 0.10
C. spinosus	Stems	< 0.001	0.0001	> 0.10
	Fronds	< 0.001	0.0001	> 0.10
Fractofusus	Length	< 0.001	0.0010	> 0.10
Plumeropriscum	Stems	< 0.001	0.0001	> 0.10
	Fronds	< 0.001	0.0001	> 0.10
Primocandelabrum	Stems	< 0.001	0.0001	< 0.01
	Fronds	< 0.001	0.0001	< 0.05
Thectardis	Cones	< 0.010	0.0001	> 0.10
				> 0.10

763

764

765 **Table 2.** Cohort analyses for each morphogroup orientation distribution. σ indicates the
766 standard deviation of each cohort with respect to the provided mean orientation. Where all
767 cohorts within a population have equal standard deviation (such as *Beothukis*) a single σ is
768 given, and where each σ varies according to the cohort (unequal variance) then a value is

769 given for each cohort. Note that the *Fractofusus* data is taken from Clapham et al. 2003. Note
770 for *C. spinosus* and *Primocandelabrum* the cohorts of one represents outliers, which were not
771 well resolved by cohort-analyses (Supp. Fig. 3).

772

Taxa	**Measured**	**N**	**Mean Orientation (°)**	**σ**	**Proportion**
Beothukis	Fronds	1	95	2.45	5.56%
		4	135		22.22%
		5	161		27.78%
		3	172		16.67%
		5	185		27.78%
Bradgatia	Fronds	30	15	26.79	57.69%
		22	188		42.31%
C. procerus	Stems	61	195	18.89	100.00%
	Fronds	61	192	30.23	100.00%
C. spinosus	Stems	30	190	30.87	96.77%
		1	326	NA	3.23%
	Fronds	30	183	24.83	96.77%
		1	328	NA	3.23%
Fractofusus	Fronds	312	172	13.19	20.84%
		678	236	26.02	45.29%
		306	295	13.44	20.44%
		201	318	5.89	13.43%
Plumeropriscum	Stems	20	178	16.73	100.00%
	Fronds	20	177	17.26	100.00%
Primocandelabrum	Stems	42	183	13.74	89.36%

		3	237	13.74	6.38%
		1	11	NA	2.13%
		1	119	NA	2.13%
	Fronds	45	187	19.05	95.74%
		1	14	NA	2.13%
		1	98	NA	2.13%
Thectardis	Cones	7	17	33.00	25.93%
		20	199		74.07%

773